Lumped-Parameter Models for Wind-Turbine Footings on Layered Ground

Andersen, Lars; Liingaard, Morten

Published in:
Proceedings of the Eleventh International Conference on Civil, Structural and Environmetal Engineering Computing

Publication date:
2007

Document Version
Publisher's PDF, also known as Version of record

Paper 227

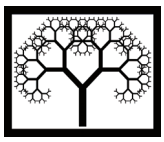

Proceedings of the Eleventh International Conference
on Civil, Structural and Environmental
Engineering Computing,
B.H.V. Topping (Editor),
Civil-Comp Press, Stirlingshire, Scotland

Lumped-Parameter Models for Wind-Turbine Footings on Layered Ground

L. Andersen[1] and M.A. Liingard[2]
[1]Department of Civil Engineering, Aalborg University, Denmark
[2]DONG Energy A/S, Fredericia, Denmark

Abstract

The design of modern wind turbines is typically based on lifetime analyses using aeroelastic codes. In this regard, the impedance of the foundations must be described accurately without increasing the overall size of the computational model significantly. This may be obtained by the fitting of a lumped-parameter model to the results of a rigorous model or experimental results. In this paper, guidelines are given for the formulation of such lumped-parameter models and examples are given in which the models are utilised for the analysis of a wind turbine supported by a surface footing on a layered ground. The importance of including an accurate model of the dynamic soil–structure interaction in an aeroelastic code is discussed. Furthermore, the sensibility of the response to changes in the soil properties is examined.

Keywords: wind turbines, foundations, impedance, dynamics, layered soil.

1 Introduction

Over the last decades, wind turbines have increased significantly in size. Optimisation of the turbine blades and towers has led to slender and therefore extremely flexible structures. Consequently, the first modes of resonance of the total structure, including the foundation (or substructure), the tower, the hub, the nacelle and the blades, are close to the excitation frequencies related to environmental loads from wind and waves. Hence, a modern wind turbine undergoes large deformations, not only during extreme weather conditions but also during power production.

Aeroelastic codes have been developed that may be employed for a lifetime analysis of the structural response. Existing codes, e.g. FLEX [1] or HAWC [2], have about 30 degrees of freedom for the entire structure including the tower, the nacelle, the hub and the rotor. However, the current models do not account for dynamic soil–structure

interaction and, as a result of this, the forces on the structure may be over- or underestimated. For example, Andersen and Clausen [3] concluded that soil stratification has a significant impact on the impedance of surface footings—even at the very low frequencies relevant to the first few modes of vibration of a wind turbine.

In this paper, the influence of the subsoil on the response of a wind turbine is discussed with focus on horizontal excitation of the structure, e.g. from wind and waves. Here, a determination of the coupled rocking and horizontal sliding impedances of the foundation is necessary and, as reported by Bu and Lin [4], various methods can be applied for this purpose. However, since computation speed is of paramount importance, the model of the foundation should only add a few degrees of freedom to the model of the structure. This may be achieved by fitting a lumped-parameter model [5] to the results of a rigorous analysis.

Firstly, a general and very stable fitting algorithm for the construction of consistent lumped-parameter models is presented, and a brief outline of the computational model for a wind turbine on a layered ground is given. Secondly, the influence of the subsoil on the response of the structure is examined. Two different sites are considered—one with a soft top layer of sand and one with a soft clay deposit at intermediate depth. The emphasis is put on the geometrical damping in the soil, and a parameter study is performed with respect to the layer depths and the material properties of the soil. To ensure realistic results, the dynamic properties of the simple model are based on field measurements on a 3 MW wind turbine in Frederikshavn, Denmark [6].

2 Model of the turbine, the footing and the subsoil

The computational model consists of two parts: a simple finite-element model of the wind turbine and a lumped-parameter model (LPM) of a rigid footing on a layered half-space, see Fig. 1. The formulation of the model has three steps:

1. A rigorous frequency-domain model is applied for the footing on a soil stratum and the frequency response is evaluated at a number of discrete frequencies.

2. A rational filter is fitted to the frequency-domain solution and an LPM providing approximately the same frequency response is calibrated.

3. The wind-turbine structure is represented by a simple finite-element model and soil–structure interaction is accounted for by a coupling with the LPM.

Figure 1 and items 1 to 3 are discussed in the subsections below, and examples of application are given in Section 3.

2.1 Rigorous model of the footing and the subsoil

The rigid footing is hexagonal with the side length r_f, the height h_f and the mass density ρ_f, see Fig. 2. This geometry is typical for offshore-wind-turbine foundations

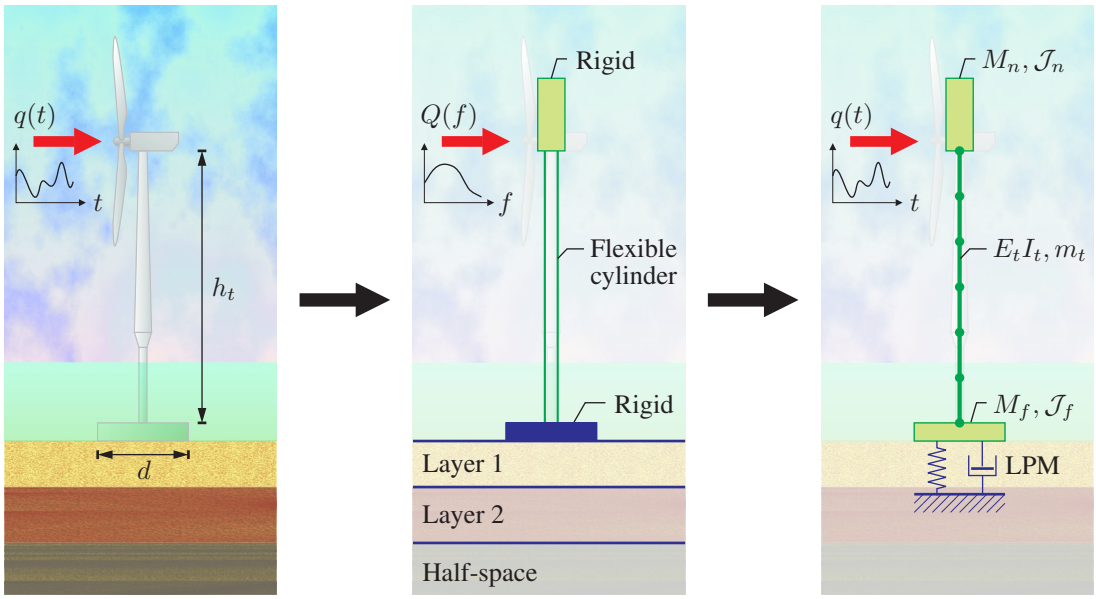

Figure 1: From prototype to computational model: Wind turbine on soil stratum (left); rigorous model of the layered half-space (centre); lumped-parameter model of the soil coupled with finite-element model of the structure (right).

and has been applied, for example, at the Nysted Offshore Wind Farm in Denmark. The centre of the soil–foundation interface coincides with the origin of the coordinate system. Hence, the mass of the foundation, M_f, and the corresponding mass moments of inertia with respect to the three coordinate axes, $\mathcal{J}_{f1}$, $\mathcal{J}_{f2}$ and $\mathcal{J}_{f3}$, become:

$$M_f = \rho_f h_f A_f, \quad \mathcal{J}_{f1} = \mathcal{J}_{f2} = \rho_f h_f \mathcal{I}_f + \frac{1}{3}\rho_f h_f^3 A_f, \quad \mathcal{J}_{f3} = 2\rho_f h_f \mathcal{I}_f. \tag{1}$$

Here A_f is the area of the horizontal cross-section and $\mathcal{I}_f$ is the corresponding geometrical moment of inertia,

$$A_f = \frac{3\sqrt{3}}{2} r_f^2, \quad \mathcal{I}_f = \frac{5\sqrt{3}}{16} r_f^4. \tag{2}$$

It is noted that $\mathcal{I}_f$ is invariant to rotation of the foundation around the x_3-axis.

The subsoil consists of two horizontal layers over a homogeneous half-space (see Fig. 2). Welded contact is assumed at all interfaces, i.e. the displacement is continuous, and the soil within each layer and the underlying half-space is considered a linear viscoelastic, homogeneous and isotropic material with the mass density ρ_j, the shear modulus μ_j and Poisson's ratio ν_j, $j = 1, 2, 3$. Hysteretic material damping with the loss factor η_j is introduced via the complex Lamé constants

$$\lambda_j^\star = \frac{2\nu_j \mu_j \left(1 + \mathrm{i}\,\mathrm{sign}(\omega)\eta^j\right)}{\left(1 - 2\nu^j\right)}, \quad \mu_j^\star = \mu_j \left(1 + \mathrm{i}\,\mathrm{sign}(\omega)\eta_j\right), \quad j = 1, 2, 3. \tag{3}$$

Here $\mathrm{sign}(\omega)$ denotes the sign of the circular frequency, ω, and subscript 3 refers to the half-space. The complex phase velocities of P- and S-waves are found as

$$c_{Pj}^\star = \sqrt{(\lambda_j^\star + 2\mu_j^\star)/\rho_j}, \quad c_{Sj}^\star = \sqrt{\mu_j^\star/\rho_j}, \quad j = 1, 2, 3. \tag{4}$$

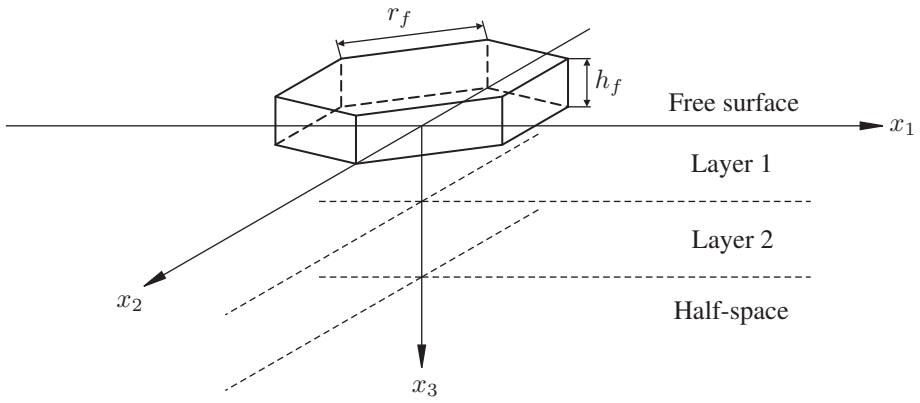

Figure 2: Hexagonal footing on a stratum with three layers over a half-space.

The surface of the ground coincides with the (x_1, x_2)-plane, see Fig. 2. In the time domain and Cartesian coordinates, the components of the surface displacement and traction are denoted $u_i(x_1, x_2, t)$ and $p_i(x_1, x_2, t)$, respectively, where $i = 1, 2, 3$. The total displacement at an observation point then becomes

$$u_i(x_1, x_2, t) = \int_{-\infty}^{t} \int_{-\infty}^{\infty} \int_{-\infty}^{\infty} g_{ij}(x_1 - y_1, x_2 - y_2, t - \tau) p_j(y_1, y_2, \tau) \, \mathrm{d}y_1 \mathrm{d}y_2 \mathrm{d}\tau, \quad (5)$$

where summation is applied over repeated indices and g_{ij} represents the fundamental solution providing the displacement in direction i at the observation point $(x_1, x_2, 0)$ and time t due to a unit force applied in direction j at the source point $(y_1, y_2, 0)$ and time τ. The spatial integral is carried out in discrete form, i.e. as a sum of the influence from L source points to a given observation point. In this process, the fundamental solution to a load distributed over a small surface area may advantageously be applied. In particular, Andersen and Clausen [7] suggested the use of a "bell-shaped" surface load in the form of a double Gaussian distribution centred at a given source point and with the standard deviation $r = r_f/\sqrt{4L}$ in both horizontal coordinate directions. Only points at the soil–foundation interface need to be considered, since the the traction on the remaining part of the ground surface is assumed to be zero. The discretization is illustrated in Fig. 3.

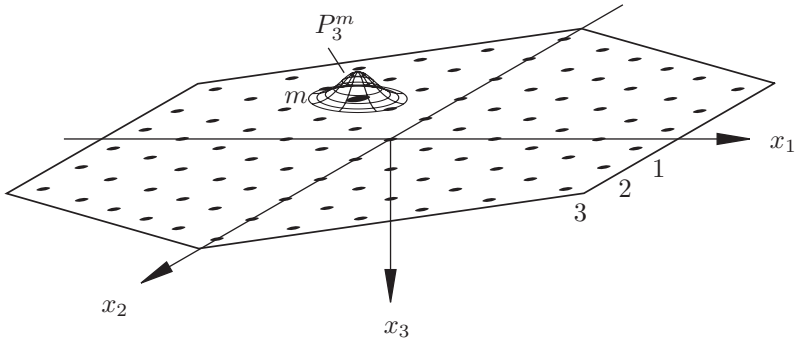

Figure 3: Discretization of the soil-foundation interface. The vertical component of the "bell-shaped" load at point m is illustrated.

In Eq. (5) it has been utilised that the response is linear and that all interfaces are horizontal. This involves that the Green's function is invariant to spatial and temporal translation and, in addition to this, a triple Fourier transformation may be carried out with regard to time and the two horizontal coordinates. This reduces the convolution provided by Eq. (5) to a set of algebraic equations,

$$\bar{U}_i(k_1, k_2, \omega) = \bar{G}_{ij}(k_1, k_2, \omega)\bar{P}_j(k_1, k_2, \omega), \tag{6}$$

that must be solved for each combination of the circular frequency ω and the horizontal wavenumbers k_1 and k_2. Whereas the Green's function g_{ij} cannot be established analytically for the stratified half-space, a closed-form solution for its triple Fourier transform $\bar{G}_{ij}(k_1, k_2, \omega)$ has been presented by, for example, Sheng et al. [8]. The surface displacements $U_i(x_1, x_2, \omega)$ in the frequency domain and spatial coordinates are established by inverse Fourier transformation of $\bar{U}_i(k_1, k_2, \omega)$ with respect to the horizontal wavenumbers. This operation becomes particularly simple when performed in polar coordinates [9, 7], which is possible with the "bell-shaped" load.

The footing has six degrees of freedom as illustrated in Fig. 4. In the frequency domain, the translations and rotations are related to the complex amplitudes of the corresponding forces and moments:

$$\mathbf{CZ} = \mathbf{F}, \tag{7a}$$

$$\mathbf{C} = \begin{bmatrix} C_{11} & 0 & 0 & 0 & C_{15} & 0 \\ 0 & C_{22} & 0 & C_{24} & 0 & 0 \\ 0 & 0 & C_{33} & 0 & 0 & 0 \\ 0 & C_{24} & 0 & C_{44} & 0 & 0 \\ C_{15} & 0 & 0 & 0 & C_{55} & 0 \\ 0 & 0 & 0 & 0 & 0 & C_{66} \end{bmatrix}, \quad \mathbf{Z} = \begin{bmatrix} V_1 \\ V_2 \\ V_3 \\ \Theta_1 \\ \Theta_2 \\ \Theta_3 \end{bmatrix}, \quad \mathbf{F} = \begin{bmatrix} Q_1 \\ Q_2 \\ Q_3 \\ M_1 \\ M_2 \\ M_3 \end{bmatrix}, \tag{7b}$$

where $\mathbf{C} = \mathbf{C}(\omega)$ is the impedance matrix. Due to the invariance of $\mathcal{I}_f$ with respect to a rotation of the footing around the x_3-axis, it follows that $C_{11} = C_{22}$, $C_{44} = C_{55}$ and $C_{15} = -C_{24}$ for the hexagonal footing. Furthermore, coupling only exists between horizontal sliding in the x_1-direction and rocking about the x_2-axis and vice versa. Each non-zero component of the impedance matrix is found by prescribing a

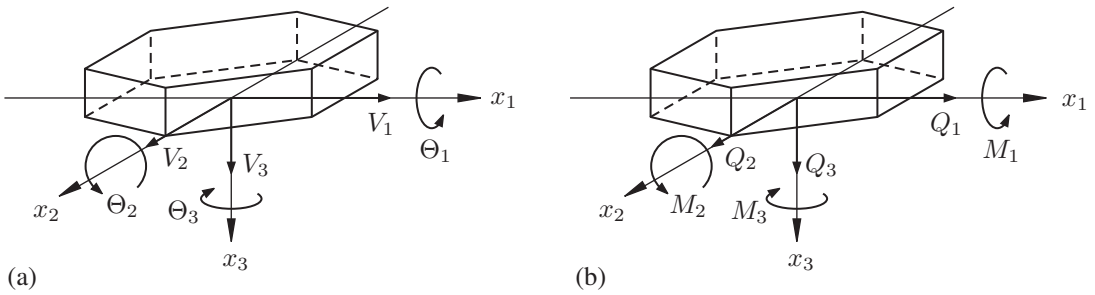

Figure 4: Degrees of freedom for a rigid surface footing: (a) displacements and rotations, and (b) forces and moments.

rigid-body motion of the footing and then solving for the unknown magnitudes of the "bell-shaped" loads. For example, $C_{33} = Q_3/V_3$, where V_3 is a prescribed vertical displacement amplitude and the corresponding force Q_3 is determined by summation of the load magnitudes P_3^m, $m = 1, 2, ..., L$, provided by the forced displacement.

2.2 Lumped-parameter model of the footing

The components of the impedance matrix may be expressed as $C_{ij}(a_0) = K_{ij}S_{ij}(a_0)$ (no sum on i, j). Here, $K_{ij} = C_{ij}(0)$ denotes the static stiffness related to the interaction of the two degrees of freedom i and j, and $a_0 = \omega r_0/c_0$ is a non-dimensional frequency with r_0 and c_0 denoting a characteristic length and wave velocity, respectively. In the present analyses, $r_0 = r_f$ and $c_0 = c_{S1}$ will be applied.

For simplicity, the subscripts i and j are omitted, i.e. $C(a_0) \sim C_{ij}(a_0)$. Then, as suggested by Wolf [5], the frequency-dependent stiffness coefficient $S(a_0)$ for a single component of the impedance matrix is decomposed into a singular part, $S_s(a_0)$, and a regular part, $S_r(a_0)$,

$$C(a_0) = KS(a_0), \qquad S(a_0) = S_s(a_0) + S_r(a_0). \tag{8}$$

K is the static stiffness component, and the singular part of the stiffness coefficient has the form

$$S_s(a_0) = k^\infty + \mathrm{i}a_0 c^\infty. \tag{9}$$

The two real constants k^∞ and c^∞ are selected so that $KS_s(a_0)$ provides the entire stiffness in the high-frequency limit $a_0 \to \infty$. For the rigid surface footing the term Kk^∞ vanishes, i.e. $k^\infty = 0$, and the complex stiffness in the high-frequency range becomes a pure mechanical impedance with

$$c_{11}^\infty = c_{22}^\infty = \frac{\rho_1 c_{S1} A_f}{K}, \quad c_{33}^\infty = \frac{\rho_1 c_{P1} A_f}{K}, \tag{10a}$$

$$c_{44}^\infty = c_{55}^\infty = \frac{\rho_1 c_{P1} \mathcal{I}_f}{K}, \quad c_{66}^\infty = \frac{2\rho_1 c_{S1} \mathcal{I}_f}{K}, \tag{10b}$$

where A_f and $\mathcal{I}_f$ are given by Eq. (2). The coupling terms $C_{15} = -C_{24}$ vanish in the high-frequency limit, i.e. there is no interaction between rocking and sliding.

The regular part $S_r(a_0)$ of the non-dimensional impedance is approximated by least-squares fitting of a rational filter to the results $S_r(a_0) = C(a_0)/K - S_s(a_0)$ obtained by the rigorous model described in the preceding subsection, i.e.

$$S_r(a_0) \approx \hat{S}_r(\mathrm{i}a_0) = \frac{\mathcal{P}(\mathrm{i}a_0)}{\mathcal{Q}(\mathrm{i}a_0)}, \tag{11a}$$

where the numerator and denominator polynomials are given as

$$\mathcal{P}(\mathrm{i}a_0) = 1 - k^\infty + p_1(\mathrm{i}a_0) + p_2(\mathrm{i}a_0)^2 + \ldots + p_{M-1}(\mathrm{i}a_0)^{M-1}, \tag{11b}$$

$$\mathcal{Q}(\mathrm{i}a_0) = \prod_{n=1}^{N} (\mathrm{i}a_0 - s_n)\,(\mathrm{i}a_0 - s_n^*) \cdot \prod_{n=N+1}^{M-N} (\mathrm{i}a_0 - s_n)\,, \tag{11c}$$

respectively. The coefficients of $\mathcal{P}(\mathrm{i}a_0)$, i.e. $p_1, p_2, ..., p_{M-1}$, are all real. Further, $2N$ roots of $\mathcal{Q}(\mathrm{i}a_0)$ appear as complex conjugate pairs: $s_n = s_n^{\Re} + \mathrm{i}s_n^{\Im}$ and $s_n^* = s_n^{\Re} - \mathrm{i}s_n^{\Im}$, $n = 1, 2, \ldots, N$, where $s_n^{\Re}$ and $s_n^{\Im}$ are the real and imaginary parts of s_n, respectively. The remaining $M - 2N$ roots of $\mathcal{Q}(\mathrm{i}a_0)$ are real.

In the present analyses, only pairs of complex conjugate roots will be utilised, i.e. the order of the rational approximation must be even. Andersen [3] argued that this provides the lumped-parameter model with the fewest possible internal degrees of freedom for a given order, M. The optimisation algorithm is given in Table 1. The coefficients of $\mathcal{P}(\mathrm{i}a_0)$ are applied as optimisation variables along with the real and imaginary parts of the complex roots of $\mathcal{Q}(\mathrm{i}a_0)$, i.e. $s_m^{\Re} = \Re(s_m)$ and $s_m^{\Im} = \Im(s_m)$, $m = 1, 2, \ldots, M/2$. Constraints of the kind $s_m^{\Re} < 0$ and $s_m^{\Im} > 0$ are included to ensure a physically valid lumped-parameter model and poles that are actually complex. Due to finite computer precision, the zeros have been replaced by a small number, $\pm\varepsilon$. Additional constraints which prevent the imaginary parts of the complex poles from being much greater than the real parts are suggested. If the real part of the complex pole s_m vanishes, i.e. $s_m^{\Re} = 0$, this results in a second order pole, $\{s_m^{\Im}\}^2$, which is real and positive. Evidently, this will lead to instability in the time domain. Since computer precision is finite, a real part of a certain size relatively to the imaginary part of the pole is necessary to ensure a stable solution.

Finally, as suggested by Wolf [5] a weight function, $w(a_0)$, has been introduced to improve the quality of the fit in the low-frequency range. In the present analyses,

$$w(a_0) = \frac{1}{(1 + (\varsigma_1 a_0)^{\varsigma_2})^{\varsigma_3}}, \tag{12}$$

where $\varsigma_1 = \varsigma_2 = \varsigma_3 = 2$. All the above-mentioned constraints have been implemented into a Fortran code based on the NLPQL optimisation algorithm [10].

The total approximation of $S(a_0)$ is found by an addition of Eqs. (9) and (11) as stated in Eq. (8). The approximation of $S(a_0)$ has two important characteristics:

- It is exact in the static limit, since $S(a_0) \approx S_s(a_0) + \hat{S}_r(\mathrm{i}a_0) \to 1$ for $a_0 \to 0$.
- It is exact in the high-frequency limit. Here, $S(a_0) \to S_s(a_0)$ for $a_0 \to \infty$, because $\hat{S}_r(\mathrm{i}a_0) \to 0$ for $a_0 \to \infty$.

Hence, the approximation is double-asymptotic, and at intermediate frequencies the quality depends on the order of the rational filter. For the considered footing on a stratum, orders from $M = 6$ to 10 have been found to provide results of an acceptable accuracy in the low-frequency range $0 - 6$ Hz. Typically, the rocking impedance may be fitted by a rational filter of lower order than the sliding and coupling impedances, especially in the case of undrained soil as indicated by the results in Section 3.

Definition: A rational filter for the regular part of the dynamic stiffness, $S_r(a_0)$, is defined in the form:

$$S_r(a_0) \approx \hat{S}_r(\mathrm{i}a_0) = \frac{\mathcal{P}(\mathrm{i}a_0)}{\mathcal{Q}(\mathrm{i}a_0)} = \frac{1 - k^\infty + p_1(\mathrm{i}a_0) + p_2(\mathrm{i}a_0)^2 + \ldots + p_{2N-1}(\mathrm{i}a_0)^{M-1}}{\prod_{m=1}^{M/2}(\mathrm{i}a_0 - s_m)(\mathrm{i}a_0 - s_m^*)}.$$

Find the optimal polynomial coefficients p_n and poles s_m which minimise the object function

$$F(p_n, s_m) = \sum_{j=1}^{J} w(a_{0j}) \left(\hat{S}_r(\mathrm{i}a_{0j}) - S_r(a_{0j})\right)^2$$

subject to the constraints $G_0(p_n, s_m), G_1(p_n, s_m), \ldots, G_{M/2}(p_n, s_m)$.

Input:	M :	order of the filter	(must be an even number),
	p_n^0,		$n = 1, 2, \ldots, M-1$,
	$s_m^{\Re 0}$,		$m = 1, 2, \ldots, M/2$
	$s_m^{\Im 0}$,		$m = 1, 2, \ldots, M/2$,
	a_{0j},		$j = 1, 2, \ldots, J$,
	$S_r(a_{0j})$,		$j = 1, 2, \ldots, J$,
	$w(a_{0j})$,		$j = 1, 2, \ldots, J$.
Variables:	p_n,		$n = 1, 2, \ldots, M-1$,
	$s_m^{\Re}$,	$s_m^{\Re} < -\varepsilon$,	$m = 1, 2, \ldots, M/2$,
	$s_m^{\Im}$,	$s_m^{\Im} > +\varepsilon$,	$m = 1, 2, \ldots, M/2$.
Constraints:	$G_0(p_n, s_m) = 1 - \prod_1^M (-s_m) = 0$,		
	$G_k(p_n, s_m) = \zeta s_k^{\Re} + s_k^{\Im} < 0$,		$k = 1, 2, \ldots, M/2$.
Output:	p_n,		$n = 1, 2, \ldots, M-1$,
	$s_m^{\Re}$,		$m = 1, 2, \ldots, M/2$,
	$s_m^{\Im}$,		$m = 1, 2, \ldots, M/2$,

Here, $s_m^{\Re} = \Re(s_m)$ and $s_m^{\Im} = \Im(s_m)$, and superscript 0 indicates initial values of the respective variables, whereas $S_r(a_{0j})$ are the "exact" values of the dynamic stiffness evaluated at the J discrete dimensionless frequencies a_{0j}, obtained by the rigorous model. Further, $\hat{S}_r(\mathrm{i}a_{0j})$ are the values of the rational filter at the same discrete frequencies, and $w(a_0)$ is a weight function. Finally, ζ and ε are two real parameters chosen as $\zeta \approx 10 \sim 100$ and $\varepsilon \approx 0.01$. Note that the initial values of the poles must conform with the equality constraint $G_0(p_n, s_m)$.

Table 1: Weighted least-squares fitting of rational filter by optimisation of the poles.

The next step in the calibration of a lumped-parameter model is to recast the polynomial-fraction form (11) of the rational approximation into partial-fraction form:

$$\hat{S}_r(\mathrm{i}a_0) = \sum_{m=1}^{M} \frac{A_m}{\mathrm{i}a_0 - s_m}. \tag{13}$$

Here A_m, $m = 1, 2, \ldots, M$, are the residues corresponding to the poles of $\hat{S}_r(\mathrm{i}a_0)$,

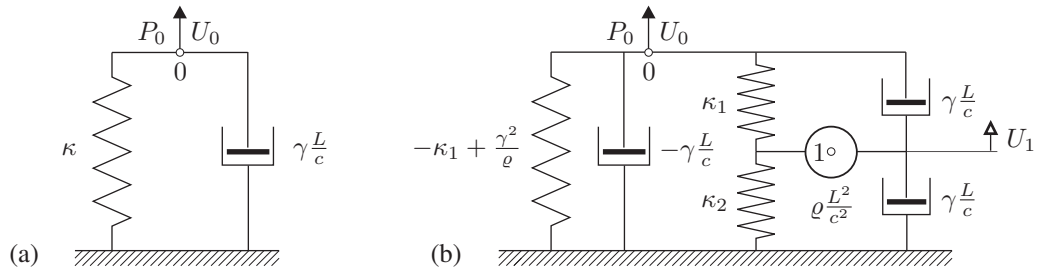

Figure 5: Discrete-element models: (a) Constant/linear term and (b) second-order term with one internal degree of freedom.

i.e. the roots s_m of $\mathcal{Q}(\mathrm{i}a_0)$. When all poles appear as complex conjugate pairs, the total approximation of the dynamic stiffness coefficient $S(a_0)$ may be written as

$$\hat{S}(\mathrm{i}a_0) = k^\infty + \mathrm{i}a_0 c^\infty + \sum_{m=1}^{M/2} \frac{\beta_{0m} + \beta_{1m}\mathrm{i}a_0}{\alpha_{0m} + \alpha_{1m}\mathrm{i}a_0 + (\mathrm{i}a_0)^2}. \tag{14}$$

The real coefficients α_{0m}, α_{1m}, β_{0m} and β_{1m} are given by

$$\alpha_{0m} = \{s_m^\Re\}^2 + \{s_m^\Im\}^2, \qquad \alpha_{1m} = -2s_m^\Re, \tag{15a}$$

$$\beta_{0m} = -2A_m^\Re s_m^\Re + 2A_m^\Im s_m^\Im, \qquad \beta_{1m} = 2A_m^\Re. \tag{15b}$$

where $A_m^\Re = \Re(A_m)$ and $A_m^\Im = \Im(A_m)$ are the real and imaginary parts of the residues which appear as complex conjugate pairs.

Referring to Eq. (14), the total approximation of the rigorous solution consists of a constant/linear term providing the singular part of the impedance, i.e. the high-frequency solution, and a number of second-order terms providing the regular part. Each of these terms may be interpreted as the frequency-response function for a so-called discrete-element model, see Fig. 5. The spring and damping coefficients as well as the point masses in these models are uniquely defined in terms of k^∞, c^∞ and the coefficients listed in Eq. (15) where, in the present case, $k^\infty = 0$. A detailed explanation may be found, for example, in the work by Wolf [5].

It is noted that the lumped-parameter model provides a real-valued impedance in the low-frequency limit, i.e. for $\omega \to 0$, since it is based on viscous dashpots. However, the hysteretic damping model defined by Eq. (3) leads to a complex impedance in the frequency domain, even in the static limit. This discrepancy leads to numerical difficulties in the fitting procedure and to overcome this, the hysteretic damping model for the soil is replaced by a linear viscous one at frequencies below 1 Hz.

2.3 Soil–structure interaction for a wind turbine on a rigid footing

As indicated by Fig. 1, the final step in the formulation of the simplified computational model of the wind turbine is to couple the LPM of the soil with a finite-element (FE)

model of the turbine structure. The aim of the present analysis is to quantify the impact of geometrical damping in the soil on the structural response and furthermore to determine the influence of the soil stiffness on the dynamic properties of the structure. Hence, the mass and the resonance frequencies of the FE model must be representative of real wind turbines.

Liingard [11] investigated the natural frequencies of a Vestas 3.0 MW offshore wind turbine located at Aalborg University's offshore test facility in Frederikshavn, Denmark. This turbine has a hub height of 80 m, a rotor diameter of 90 m and an operational interval of 8.6 to 18.4 rounds per minute. The weight of the nacelle, the rotor and the tower are 70 t, 41 t and 160 t, respectively. Further details can be found in [12]. The structure is supported by a suction caisson with a diameter of 12 m and a skirt length of 6 m. The weight of the suction caisson is approximately 140 t. The foundation and the structure were equipped with an online monitoring system, consisting of 15 accelerometers and a real-time data-acquisition system. This system has been used for "output-only modal identification" of the natural frequencies of the wind turbine, employing the software package ARTeMIS [13].

In Fig. 6, the output of the modal analysis is shown, based on data recorded on February 15, 2005 over a one-hour period and with the sampling frequency 200 Hz. The analysis has been carried out for idle conditions to avoid interference caused by rotating components of the wind turbine. More specifically, the plot shows the frequency-dependent singular values of the spectral density matrix (SVSDM) for one of the accelerometers, determined by the Frequency-Domain Decomposition method [14, 15]. The peaks corresponding to the first and second tower mode have been identified at 0.30 Hz and 2.13 Hz, respectively. The peaks between the first and second mode of the wind turbine correspond to the resonance frequencies of the blades, i.e. the first modes of flap-wise and edgewise vibrations. The peak at 2.93 Hz appears to be a torsional mode of the structure. No significant excitations appear above 5 Hz at idle conditions, and for that reason the frequency range of interest is between 0 and 5 Hz for the structural analyses.

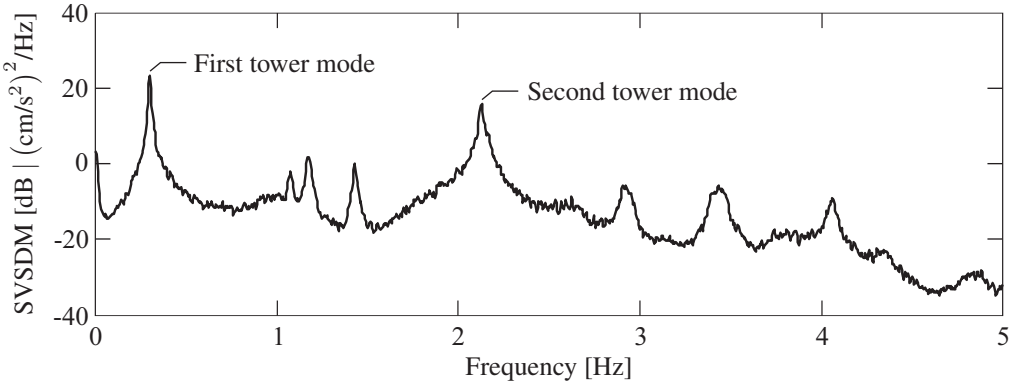

Figure 6: Singular values of the spectral density matrix (SVSDM) for an accelerometer determined by the Frequency-Domain Decomposition method at idle conditions.

In the present analysis, a wind turbine with similar properties is considered. The tower (including the substructure from the base of the tower down to the foundation) is modelled as a circular steel tube with an outer diameter of 6 m, a material thickness of 20 mm, a Young's modulus of $E_t = 200$ GPa and mass density of 8500 kg/m^3. The high mass density reflects the fact that not all the material contributes to the stiffness. The height of the tower is $h_t = 120$ m, and six Euler-Bernoulli beam elements are applied for the discretization of the flexural behaviour, see Fig. 1. The mass per unit length, m_t, and the bending stiffness, $E_t I_t$, are readily obtained from the geometry and the material properties of the tower. The vertical and torsional vibrations are disregarded and, with reference to Fig. 1, only the in-plane horizontal displacements and rotations are considered. At the base of the tower, these are coupled via rigid massless beam elements to the lumped-parameter models for the sliding and rocking motion of the the footing. The mass and the mass moments of inertia of the footing are defined by Eqs. (1)–(2) with $\rho_f = 2000$ kg/m^3, $h_f = 5$ m and $r_f = 10$ m.

Finally, the nacelle, the hub and the rotor blades are simply included as a rigid body with the mass $M_n = 150.000$ kg and the corresponding in-plane mass moment of inertia $\mathcal{J}_n = 4.500.000$ kg·m^4 measured about the axes through the top node of the FE model of the turbine tower. In reality, the blades of a modern wind turbine are extremely flexible, as indicated by the relatively low resonance frequencies of about 1–1.5 Hz (the three spikes between the 1st and 2nd mode in Fig. 6). However, according to Fig. 6 and the explanation given above, the primary response at the base of the turbine is related to the first and second tower mode. Even the simple model will provide an acceptable accuracy of the frequencies f_1 and f_2 related to these modes of resonance. In particular, for a turbine fixed at the base the FE model provides the frequencies $f_1 = 0.30$ Hz and $f_2 = 2.3$ Hz. Lower values are obtained when soil–structure interaction is taken into account as further discussed in the next section.

Finally it is noted that the finite-element model of the wind turbine does not account for any damping—neither structural damping nor aerodynamic damping. In addition to this, the parametric excitation of the system stemming from rotating parts of the turbine (primarily the rotor) are not included in the simple model. A slightly more realistic model may be obtained by the inclusion of aerodynamic and structural damping, e.g. by means of a Rayleigh-damping model; but an aeroelastic code is required for the design and analysis of turbines. However, the present analysis focuses on a determination of the geometrical damping in the soil with emphasis on the two first tower modes, and for this purpose the simple FE model will suffice.

3 Influence of soil properties on the dynamic response

The computational model is applied for the analysis of a wind turbine on layered soil at two different sites, one site with a top layer of loose sand and another site with a soft clay deposit at intermediate depth. The soil profiles are based on actual data from planned offshore wind farms in the British territorial waters. However, the specific position of the sites is confidential.

3.1 A top layer of soft sand on an over-consolidated clay deposit

The soil at the first site consists of a top layer of loose sand with a depth of 6 to 12 m overlying a 20 m deep layer of pre-consolidated clay. A slightly stiffer clay deposit constitutes the half-space underneath. As indicated in Table 2, the sand in the top layer is assumed to be fully drained (D) or undrained (U), whereas the clay is considered undrained in all the analyses.

Figure 7 shows the frequency response related to the horizontal displacement $v(t)$ and the corresponding rotation $\theta(t)$ at the hub for $h_1 = 6$ m and $\mu_1 = 5$ MPa (drained sand). $H_{vv}^{-1}(f)$ and $H_{\theta\theta}^{-1}(f)$ are the diagonal terms of the frequency-response matrix

$$\mathbf{H}^{-1}(f) = \left(\mathbf{K} + 2\pi \mathrm{i} f \mathbf{C} - 4\pi^2 f^2 \mathbf{M}\right)^{-1}, \tag{16}$$

where $\mathbf{K}$, $\mathbf{C}$ and $\mathbf{M}$ are the stiffness, damping and mass matrices obtained by assembly of the finite-element and lumped-parameter models. A comparison with the results achieved for a structure fixed at the base (the dashed lines) indicates that the first resonance frequency is lowered from 0.30 Hz to 0.23 Hz, whereas the second resonance frequency has changed from 2.27 Hz to 1.70 Hz after the inclusion of the soil.

Layer no.	Soil type	h (m)	μ (MPa)	ν	ρ (kg/m^3)	η
Layer 1a	Soft sand (D)	6 / 12	5 / 10	0.250	1500	0.03
Layer 1b	Soft sand (U)	6 / 12	5 / 10	0.497	2000	0.03
Layer 2	Stiff clay	28	25	0.497	2000	0.02
Half-space	Hard clay	∞	50	0.497	2100	0.01

Table 2: Material properties for the layered half-space at Site No. 1.

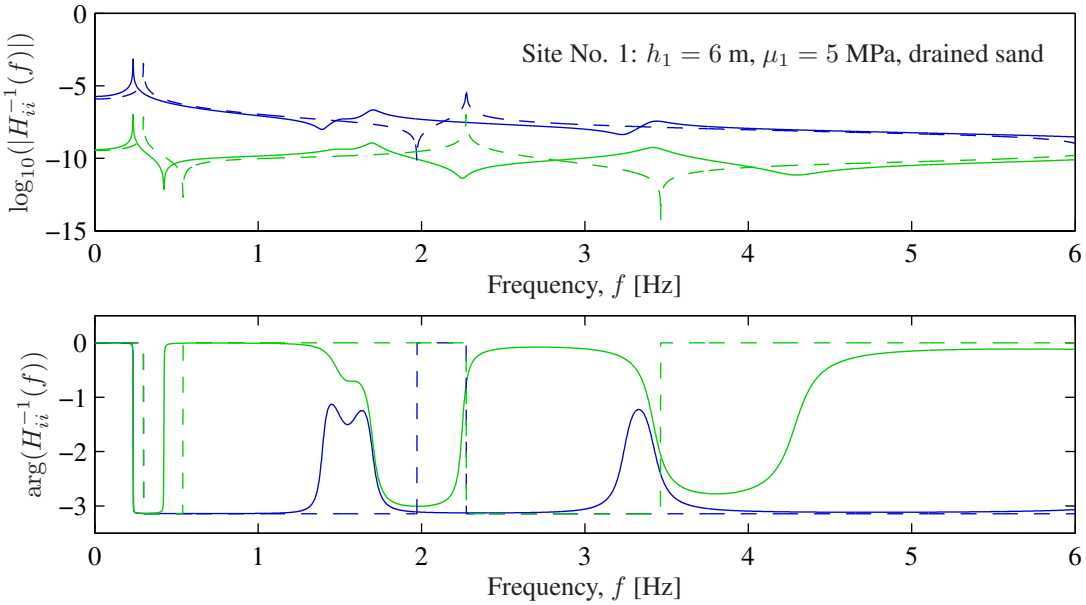

Figure 7: Frequency response at the hub. The full lines indicate results for the soil–structure-interaction problem: $H_{vv}^{-1}(f)$ (——); $H_{\theta\theta}^{-1}(f)$ (——). The dashed lines show the results for a turbine fixed at the base: $H_{vv}^{-1}(f)$ (– –); $H_{\theta\theta}^{-1}(f)$ (– –).

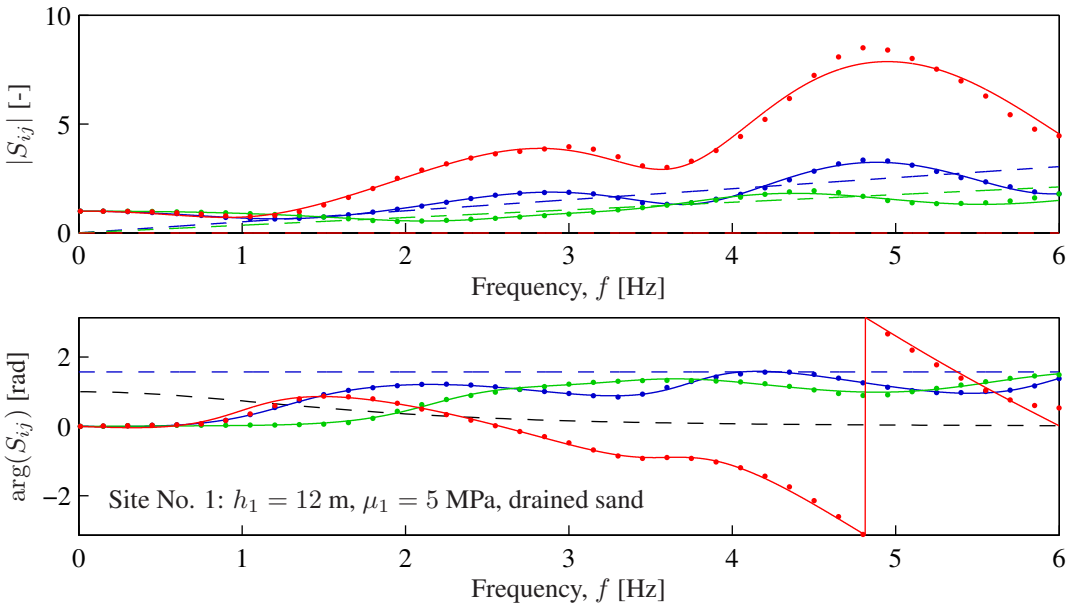

Figure 8: Dynamic stiffness coefficient obtained by lumped-parameter models: S_{11} (——), S_{55} (——) and S_{15} (——). The dots depict the corresponding target results of the rigorous model and the dashed lines show the high-frequency solution. Finally, the black dashed line (– –) indicates the weight function w (not in radians).

The frequency response of the wind turbine on the hexagonal footing over the layered half-space indicated by the full lines in Fig. 7 has been obtained with lumped-parameter models of the order $M = 10$ for the horizontal sliding and coupling terms, i.e. S_{11} and S_{15}. However, the rocking impedance has been fitted by a 6th-order filter. As shown in Fig. 8, this provides an accurate match to the target results for $h_1 = 12$ m and $\mu_1 = 5$ MPa (drained sand), and a similar conclusion can be made for other properties of the layered ground. However, additional studies show that the behaviour of the layered half-space is not correctly described by low-order models, i.e. second or fourth order models. It is noted that additional points have been included in the least-squares optimisation beyond the maximum frequency in the rigorous solution. The regular part of the normalised impedance at these points has been put equal to zero in order to obtain a lumped-parameter model that rapidly approaches the high-frequency solution. For some combinations of the material properties and layer depths, this has been useful in order to avoid unstable solutions in the time domain.

Next, a concentrated horizontal force is applied at the hub which is placed two metres above the top of the tower. The force is a narrow-banded pulse of the kind

$$q(t) = \begin{cases} \sin(2\pi f_c t)\sin(\pi f_c t/3) & \text{for} \quad 0 < t < 3/f_c, \\ 0 & \text{otherwise.} \end{cases} \tag{17}$$

A centre frequency of $f_c = 3$ Hz is selected so that both the first and the second tower mode are excited. Newmark integration [16] is applied over time, and the results obtained for $h_1 = 6$ m and different material properties of the sand are shown in Fig. 9. Similarly, the results for $h_1 = 12$ m are given in Fig. 10.

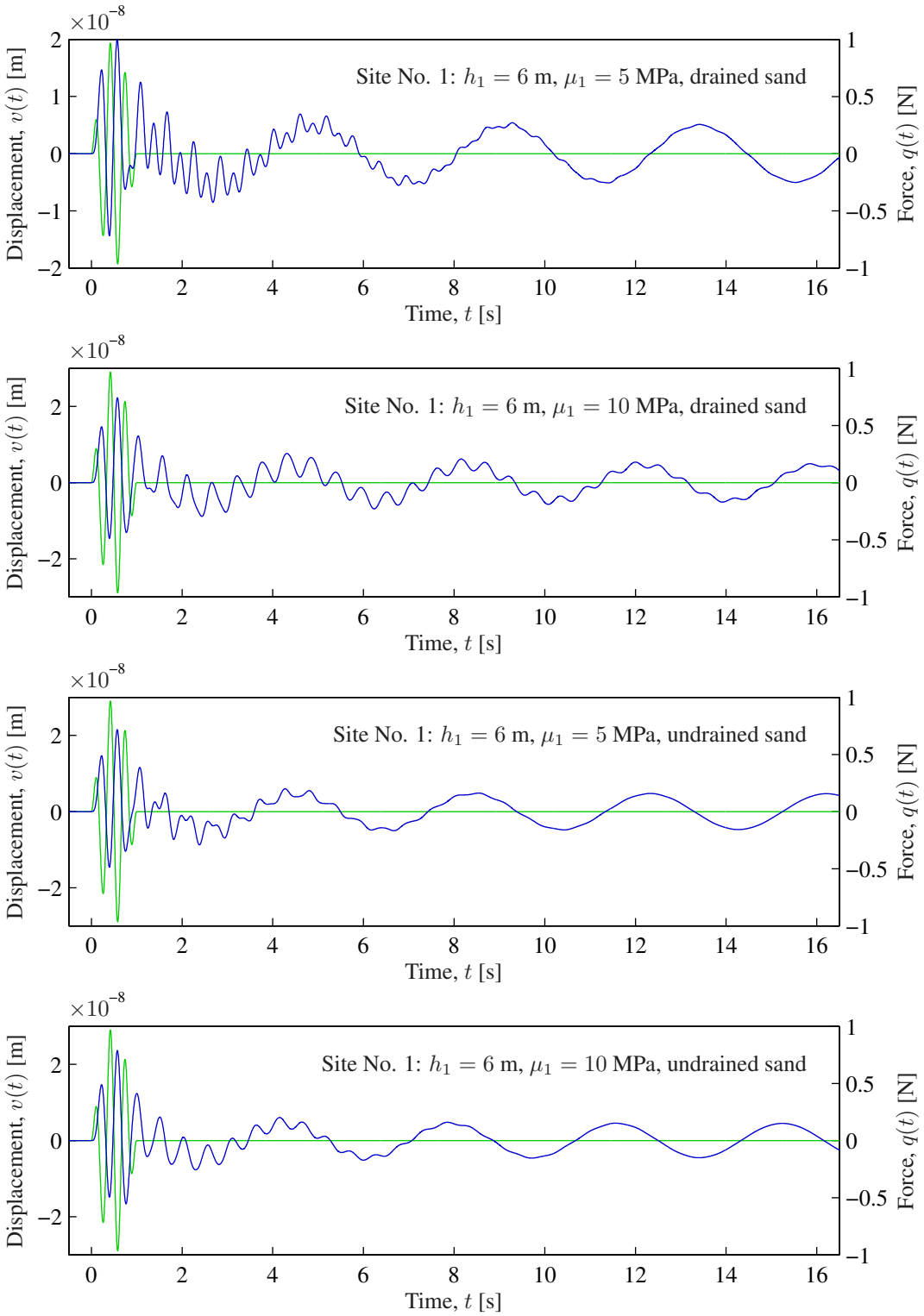

Figure 9: Horizontal displacement, $v(t)$, at the hub (——) due to a concentrated horizontal force, $q(t)$, applied at the same position (——).

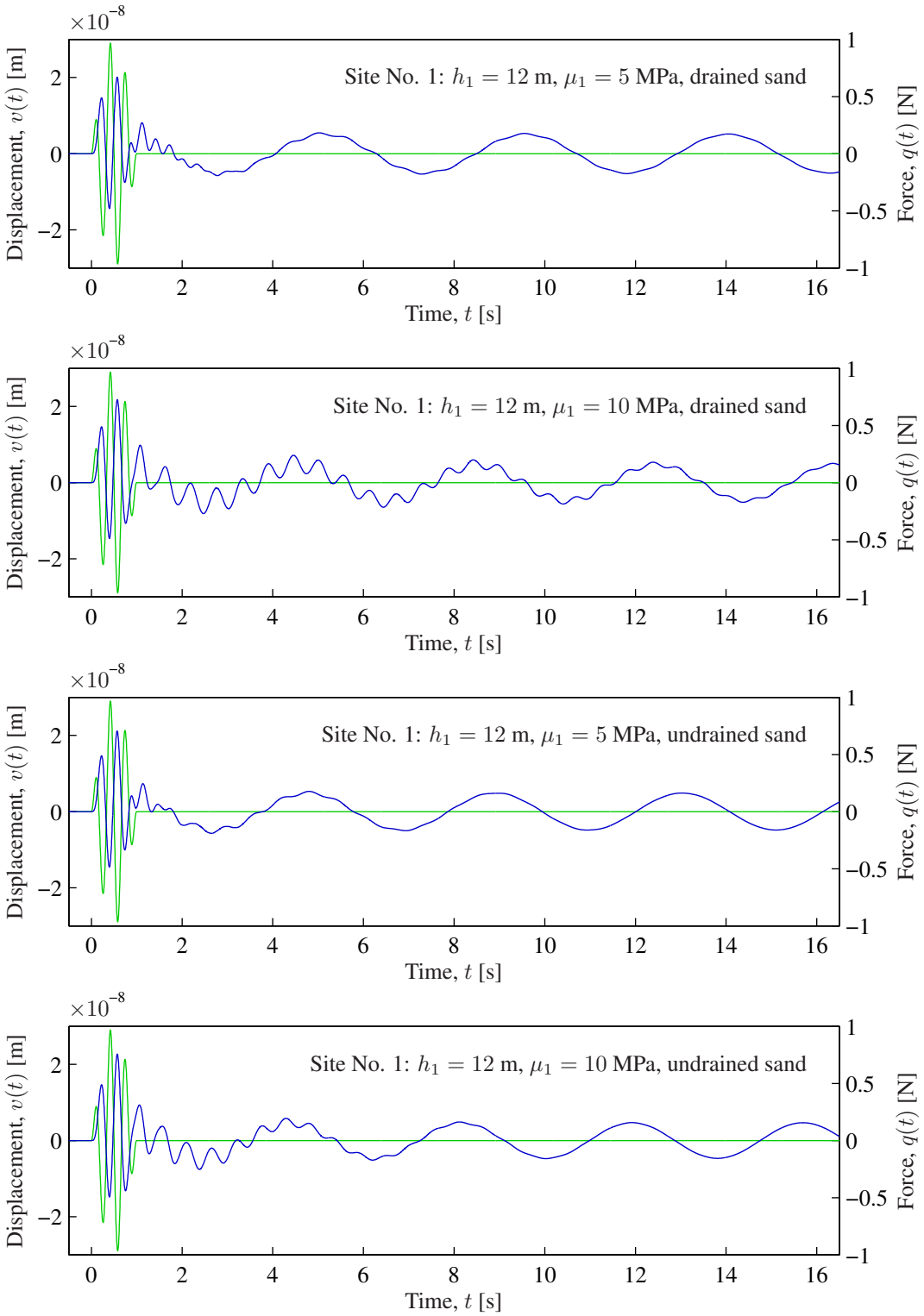

Figure 10: Horizontal displacement, $v(t)$, at the hub (——) due to a concentrated horizontal force, $q(t)$, applied at the same position (——).

Inspection of Figs. 9 and 10 leads to the conclusion that the properties of the soil have a strong influence on the structural response. As expected, both the first and the second mode of resonance are excited, and the resonance frequencies depend on the stiffness and the depth of the sand layer. This can be seen by the variation of the vibration periods during the free response after the pulse load has ended. In the case of $h_1 = 5$ m, $\mu_1 = 5$ MPa and drained conditions in the sand, vibrations occur in the third mode of resonance. In this case, Fig. 7 indicates that f_3 is about 3.5 Hz, i.e. close to the centre frequency $f_c = 3$ Hz of the pulse load.

In all the sub-figures of Figs. 9 and 10 it is observed that the second (and third) mode of the tower is damped. Since no material or aerodynamic damping is present in the structure, and almost no material damping exists in the soil, this is due to geometrical dissipation in the layered ground. The damping of the second mode is particulary strong for $h_1 = 12$ m and $\mu_1 = 5$ MPa (both drained and undrained conditions). This may be explained by the fact that the cut-on frequency, f_{co}, for wave propagation in the layered half-space is much lower than f_2 in this case, whereas f_{co} is only slightly lower than f_2 for $h_1 = 6$ m and $\mu_1 = 10$ MPa and drained sand. In any case, the cut-on frequency is higher than the first resonance frequency, which explains that first vibration mode of the tower is practically undamped.

Finally, a significant difference between the response of the turbine on drained and undrained sand is observed—especially when the sand layer is 10 m deep. Hence, it may be necessary to examine carefully whether the material is drained or undrained, and eventually a poroelastic model may be required as proposed by Biot [17].

3.2 A normally consolidated clay deposit at intermediate depth

The soil at the second site consists of a top layer of medium dense sand with a depth of 5 to 20 m overlaying a 20 m deep layer of soft normally consolidated clay and a half-space of hard clay. Detailed information is provided in Table 3.

Figure 11 shows the frequency response at the top of the turbine for $h_1 = 5$ m and $\mu_2 = 16$ MPa. Again, lumped-parameter models of the orders 10 and 6 have been applied. In this case the first resonance frequency is lowered from 0.30 Hz to 0.27 Hz, whereas f_2 has changed from 2.3 Hz to 1.9 Hz after the introduction of the LPM.

The pulse load defined by Eq. (17) is now applied to the turbine and the transient response is plotted in Fig. 12 for $h_1 = 5$ m and three different values of the shear modulus μ_2. Similarly, the results for $h_1 = 20$ m are given in Fig. 13.

Layer no.	Soil type	h (m)	μ (MPa)	ν	ρ (kg/m^3)	η
Layer 1	Medium sand	5 / 20	20	0.250	1600	0.03
Layer 2	Soft clay	20	1 / 16	0.497	1900	0.02
Half-space	Hard clay	∞	100	0.497	2200	0.01

Table 3: Material properties for the layered half-space at Site No. 2.

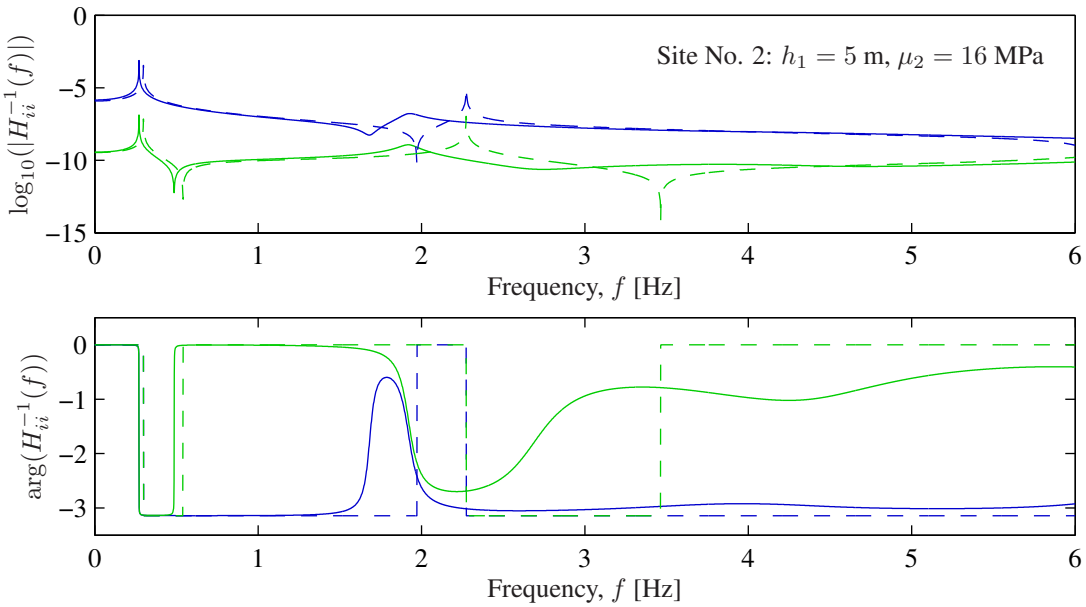

Figure 11: Frequency response at the hub. The full lines indicate results for the soil–structure-interaction problem: $H_{vv}^{-1}(f)$ (——); $H_{\theta\theta}^{-1}(f)$ (——). The dashed lines show the results for a turbine fixed at the base: $H_{vv}^{-1}(f)$ (– –); $H_{\theta\theta}^{-1}(f)$ (– –).

Analogously to the previous case with the wind turbine at Site No. 1, the second mode is strongly damped whereas the free vibrations at the first natural frequency of the turbine are nearly undamped. However, for $h_1 = 5$ m and $\mu_2 = 1$ MPa, geometrical dissipation occurs in the first mode, indicating that the cut-on frequency of wave propagation in the stratum is very low in this case, i.e. close to the first resonance frequency of the structure.

As expected, f_1 decreases when the stiffness of the clay layer becomes smaller. The change is significant when the sand layer is only 5 m deep. In this case, the sand layer acts like a plate on the much softer clay deposit. However, the difference between the resonance frequencies is much less significant for $h_1 = 20$ m, see Fig. 13. Actually, the transient response is almost identical for all simulations with the deep sand layer, independently of the stiffness of the clay. This indicates that a soil layer situated at a depth greater than the characteristic length of the foundation has very little impact on the impedance. In other words, the structure cannot "feel" the clay layer at the relatively great depth of 20 m below the ground surface. This is a disadvantage with respect to the geometrical dissipation of energy in the second tower mode. Thus, a comparison of Figs. 12 and 13 shows that the vibrations at the frequency f_2 decay more rapidly for $h_1 = 5$ m than for $h_1 = 20$ m, regardless of the clay stiffness. However, the maximum response is approximately the same for all combinations of h_1 and μ_2. Based on this, a small depth of the top layer may actually be preferred.

Finally, comparing Figs. 9, 10, 12 and 13 it is observer that the magnitude of the response at Site No. 1 and Site No. 2 is the almost identical in all situations. The most significant geometrical damping occurs at Site No. 2 with $h_1 = 5$ m. However, the weaker geometrical dissipation also occurs at Site No. 2, but for $h_1 = 20$ m.

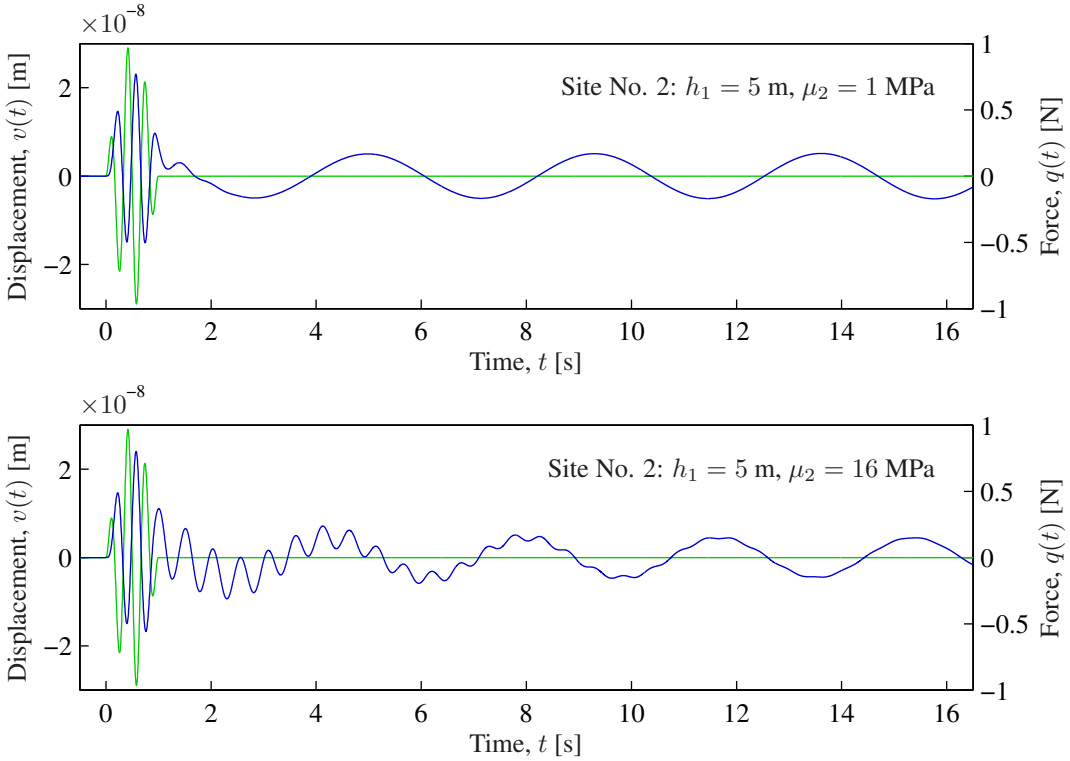

Figure 12: Horizontal displacement, $v(t)$, at the hub (——) due to a concentrated horizontal force, $q(t)$, applied at the same position (——).

4 Conclusion

The purpose of the analyses in the present paper is to assess the influence of the subsoil on the response of an offshore wind turbine. The aim of the work has been to quantify the impact of geometrical damping in the soil on the structural response and to determine the influence of the soil stiffness on the dynamic properties of the structure.

The computational model employed in the analyses consists of a simple finite-element model of the wind turbine coupled with a lumped-parameter model (LPM) of a rigid hexagonal footing on a layered half-space. The LPM is calibrated by weighted least-squares fitting of the frequency response obtained from a rigorous frequency-domain model of the footing on a soil stratum. Lumped-parameter models of the order 6 to 10 have been found to provide accurate results, whereas low-order models are not useful for the layered half-space. To ensure realistic results, the dynamic properties of the simple finite-element model are based on field measurements on a 3 MW wind turbine in Frederikshavn, Denmark.

The transient structural response due to a narrow-banded pulse load is examined. The load is applied horizontally at hub height and with a centre frequency of 3 Hz. Two different soil profiles are included in the study. Case 1 concerns a top layer of loose sand above stiff clay, and it has been found that the properties of the topsoil have a strong influence on the structural response, given by the fact that the first and second

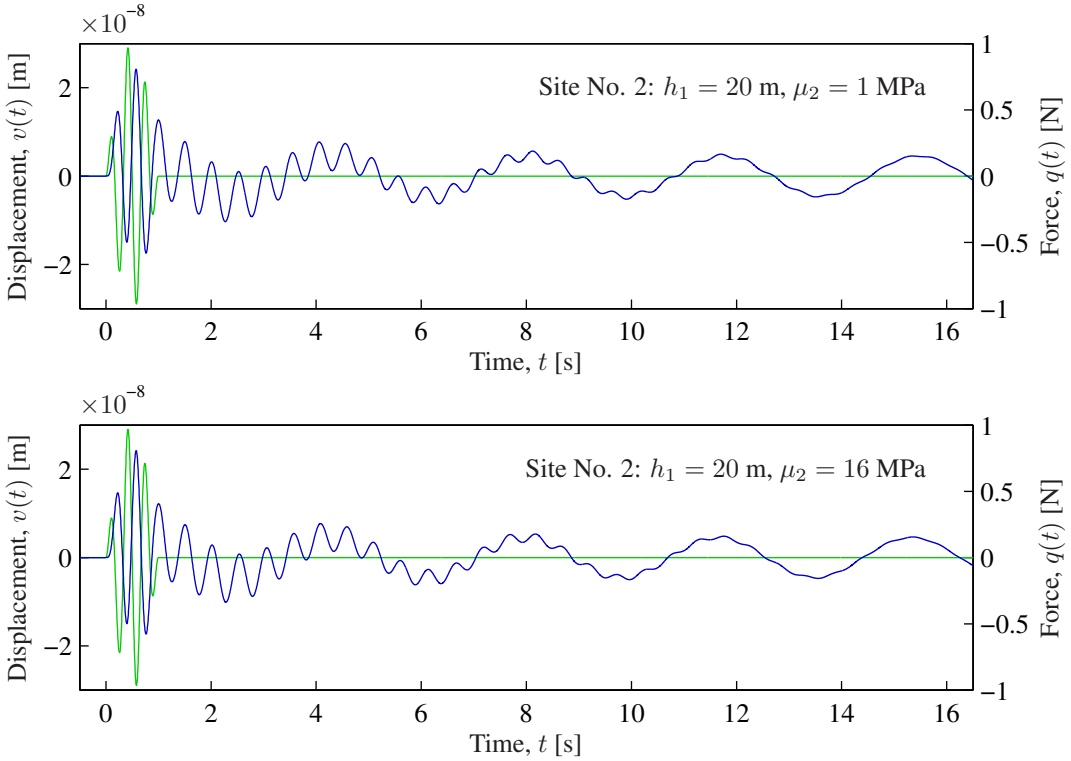

Figure 13: Horizontal displacement, $v(t)$, at the hub (——) due to a concentrated horizontal force, $q(t)$, applied at the same position (——).

resonance frequencies are lowered significantly, i.e. from 0.30 Hz to 0.23 Hz and from 2.27 Hz to 1.70 Hz, respectively. The resonance frequencies depend on the stiffness as well as the layer depth of the sand. The second mode of the tower is damped by geometrical dissipation in the ground, in particular with low stiffness and large depth of the sand layer. However, no such damping is observed with regard to the first tower mode, since the first resonance frequency is lower than the cut-on frequency of wave propagation in the stratum. Finally, a significant difference between the response of the turbine on drained and undrained sand is observed. In order to assess whether the general loading of an offshore wind turbine excites the subsoil under drained or undrained conditions, eventually a poroelastic model may be required.

Case 2 concerns a soft normally consolidated clay below a top layer of medium dense sand. By inclusion of the subsoil in the computational model, the first resonance frequency is lowered from 0.30 Hz to 0.27 Hz, whereas the second resonance frequency has changed from 2.3 Hz to 1.9 Hz. Again, the second mode is strongly damped, whereas the free vibrations at the first natural frequency of the turbine are nearly undamped. Therefore, the inclusion of an LPM in an aeroelastic code is particularly important with regard to an assessment of the resonance frequencies and the geometrical damping of the structural vibrations except for the first tower mode.

In the case of a relatively thin sand layer (5 m) above the soft clay, the sand layer acts like a plate on the much softer clay deposit. For a deep sand layer (20 m) the

transient response is almost independent of the stiffness of the clay, i.e. the structure cannot "feel" the clay layer. However, this results in very low geometrical dissipation of energy through the soft clay deposit. This observation leads to the conclusion that a small depth of the top layer may actually be preferred with respect to reducing the oscillations related to the second mode of vibration.

References

[1] S. Øye. "FLEX4 – Simulation of wind turbine dynamics", in "State of the Art of Aeroelastic Codes for Wind Turbine Calculations", B.M. Pedersen (Editor), pages 71–76, Lyngby, Denmark, 1996.

[2] T.J. Larsen and A.M. Hansen. "Aeroelastic effects of large blade deflections for wind turbines", in "The Science of Making Torque from Wind", pages 238–246, Roskilde, Denmark, 2004.

[3] L. Andersen. "Do lumped-parameter models provide the correct geometrical damping?", in "Proceedings of Computational Mechanics in the UK: 2007", B.H.V. Topping (Editor), Glasgow, Scotland, 2–3 April 2007.

[4] S. Bu and C.H. Lin, "Coupled horizontal–rocking impedance functions for embedded square foundations at high frequency factors", Journal of Earthquake Engineering, 3(4), 561–587, 1999.

[5] J.P. Wolf, "Foundation vibration analysis using simple physical models", Prentice-Hall, Englewood Cliffs, NJ, 1994.

[6] L.B. Ibsen and M. Liingaard. "Output-only modal analysis used on new foundation concept for offshore wind turbine", in "Proceedings of the 1st International Operational Modal Analysis Conference (IOMAC)", Copenhagen, Denmark, 27 April 2005.

[7] L. Andersen and J. Clausen. "Impedance of surface footings on layered ground", in "Proceedings of the Tenth International Conference on Civil, Structural and Environmental Engineering Computing", B.H.V. Topping (Editor), Stirling, United Kingdom, 2005, Civil-Comp Press, Paper 255.

[8] X. Sheng, C.J.C. Jones and M. Petyt, "Ground vibration generated by a harmonic load acting on a railway track", Journal of Sound and Vibration, 225(1), 3–28, 1999.

[9] L. Auersch, "Wave propagation in layered soils: Theoretical solution in wavenumber domain and experimental results of hammer and railway traffic excitation", Journal of Sound and Vibration, 173(2), 233–264, 1994.

[10] K. Schittkowski, "NLPQL: A fortran subroutine for solving constrained nonlinear programming problems", Annals of Operations Research, 5, 485–500, 1985/86.

[11] M. Liingaard, "DCE Thesis 3: Dynamic behaviour of suction caissons", Ph.D. thesis, Department of Civil Engineering, Aalborg University, Denmark, 2006.

[12] Vestas. "Vestas V90—3.0 MW". Vestas wind energy systems, Randers, Denmark, Brochure, downloaded at www.vestas.com, 2006.

[13] SVS. “ARTeMIS software - version 3.5”. Structural Vibration Solutions (SVS) ApS, Novi Science Park, Niels Jernes Vej 10, DK 9220 Aalborg East, Denmark, www.svibs.com, 2006.

[14] R. Brincker, P. Andersen and L. Zhang. “Modal identification from ambient responses using frequency domain decomposition”, in “Proceedings of the 18th International Modal Analysis Conference (IMAC)”, pages 625–630, San Antonio, Texas, 2000.

[15] R. Brincker, L. Zhang and P. Andersen. “Output-only modal analysis by frequency domain decomposition”, in “Proceedings of the ISMA25 Noise And Vibration Engineering”, volume 11, pages 717–723, Leuven, Belgium, September 13–15 2000.

[16] N.M. Newmark, “A method of computation for structural dynamics”, ASCE Journal of the Engineering Mechanics Division, 85(EM3), 67–94, 1959.

[17] MA Biot, “Theory of propagation of elastic waves in a fluid-saturated porous solid. I. Low-frequency range”, The Journal of the Acoustical Society of America, 28(2), 168–178, 1956.